A first look at dust lifting and dust storms near the south pole of Mars with a mesoscale model

Anthony D. Toigo[1] and Mark I. Richardson
Division of Geological and Planetary Sciences, California Institute of Technology, Pasadena, California, USA

R. John Wilson
NOAA/Geophysical Fluid Dynamics Laboratory, Princeton, New Jersey, USA

Huiqun Wang and Andrew P. Ingersoll
Division of Geological and Planetary Sciences, California Institute of Technology, Pasadena, California, USA

Received 5 September 2001; revised 30 January 2002; accepted 9 April 2002; published 12 July 2002.

[1] Surface wind stresses and dust lifting in the south polar region of Mars are examined with a three-dimensional numerical model. The focus of this study is the middle to late southern spring period when cap-edge dust lifting events are observed. Mesoscale model simulations of high southern latitudes are conducted at three dates within this season (L_s = 225°, 255°, and 310°). Assuming that dust injection is related to the saltation of sand-sized grains or aggregates, the Mars MM5 mesoscale model predicts surface wind stresses of sufficient strength to initiate movement of sand-sized particles (~100 μm), and hence dust lifting, during all three periods. The availability of dust and/or sand-sized particles is not addressed within this study. Instead, the degree to which the existence of sufficiently strong winds limit dust injection is examined. By eliminating forcing elements from the model, the important dynamical modes generating high wind stresses are isolated. The direct cap-edge thermal contrast (and topographic slopes in some locations) provides the primary drive for high surface wind stresses at the cap edge, while sublimation flow is not found to be particularly important, at these three dates. Simulations in which dust is injected into the lowest model layer when wind stresses exceed a threshold show similar patterns of atmospheric dust to those seen in recent observations. Comparison between these simulations and those without active dust injection shows no signs of consistent positive or negative feedback due to dust clouds on the surface wind stress fields during the late spring season examined here. *INDEX TERMS:* 3329 Meteorology and Atmospheric Dynamics: Mesoscale meteorology; 3346 Meteorology and Atmospheric Dynamics: Planetary meteorology (5445, 5739); 3349 Meteorology and Atmospheric Dynamics: Polar meteorology; 5445 Planetology: Solid Surface Planets: Meteorology (3346); 6225 Planetology: Solar System Objects: Mars; *KEYWORDS:* Mars, mesoscale, atmosphere, dynamics, dust, polar cap

1. Introduction

[2] The mechanisms by which dust is lifted from the surface and injected into the Martian atmosphere are currently not well understood. Numerous suggestions have been advanced on the basis of either observations or theory. These fall into essentially two categories: free (thermal) convection and large-scale winds (forced convection). The former category includes small-scale convective activity (such as dust devils) [*Gierasch and Goody*, 1973; *Thomas and Gierasch*, 1985; *Metzger et al.*, 1999; *Renno et al.*, 2000], while the latter category includes winds associated with baroclinic storm systems, slopes, etc. [*Leovy et al.*, 1973; *Peterfreund and Kieffer*, 1979; *James et al.*, 1999].

[3] However, three-dimensional numerical models to date have not been successful in generating winds (and specifically surface wind stresses, the force per unit area imposed by wind drag on the surface) of sufficient strength to initiate significant dust lifting via saltation of sand if laboratory estimates of the threshold wind stress are accepted [*Anderson et al.*, 1999; *Murphy*, 1999]. Sand-sized particles (of ~100 μm diameter) are the first particles to be mobilized on the surface. Saltation of sand has the effect of "kicking" dust into the atmosphere as the sand-sized particles impact the dust [*Greeley and Iversen*, 1985]. Alternatively, aggregates of dust that have cohered into sand-sized particles can be mobilized with similar wind stresses and collisionally disintegrate back into dust [*Greeley*, 1979]. Since sand-sized particles require the lowest threshold wind stress for mobilization, this has been a favored mechanism for dust injection

[1]Now at Center for Radiophysics and Space Research, Cornell University, Ithaca, New York, USA.

0148-0227/02/2001JE001592

in the literature. Direct lofting of dust-sized particles requires much higher surface stresses [*Greeley et al.*, 1992]. However, dust lifting via mobilization of sand-sized particles requires the presence of either sand-sized aggregates or both dust and sand particles. In this study the availability of sand-sized particles is not addressed. Instead, it is assumed either their availability or significant reductions in the required threshold stress to initiate direct injection of dust (i.e., differences between laboratory conditions and Martian conditions, such as low static stability and electrostatic forces [*Greeley et al.*, 1992]). In any case, it is assumed that sufficient wind stress for sand saltation is the limiting factor (which will not always be true), and we specifically examine the dynamical processes involved in generating high wind stresses.

[4] One particular area of interest with respect to dust lifting has been the polar cap edge region, in which strong thermal contrasts exist which are expected to generate strong winds in analogy to terrestrial sea breeze circulations. These winds may be augmented by flow due to the sublimation of CO_2 and by the presence of steep slopes in the vicinity of the polar layered terrain, the residual cap, or the seasonal cap edge [*Burk*, 1976; *Haberle et al.*, 1979; *Siili et al.*, 1997, 1999]. The interest in the polar cap edge emerges not only from theoretical considerations but also from observations of dust activity in these regions [*Kahn et al.*, 1992].

[5] Even in the strongly forced polar regions, general circulation models have been unable to generate significant areas where the laboratory-measured wind stress threshold for mobilization of sand-sized particles is exceeded [*Anderson et al.*, 1999; *Murphy*, 1999]. There are three potential reasons for this. First, global-scale models may not possess sufficient horizontal resolution to properly simulate the important circulation systems. Second, while higher-resolution mesoscale models have been applied to cap edge and slope winds, these models have been two-dimensional and have not included all the dynamical processes of potential importance [*Siili et al.*, 1997, 1999]. Third, the laboratory-measured wind stress thresholds may be unrealistically high for the true Martian environment (due to not accounting for unstable atmospheric conditions and electrostatic forces).

[6] The study of dust lifting by a variety of processes and at a variety of locations must be undertaken to fully understand the dust cycle on Mars and how dust is injected into the atmosphere. However, this is too large a question to attack in one study alone. Thus, as a first step toward answering this question, focus was placed on both a particular mechanism favored in the literature and a particular location of known dust activity. In this study, focus was placed on the development of cap edge storms along the retreating edge of the southern spring polar cap. It is assumed that dust lifting is controlled by mobilization of sand-sized particles, that the threshold for mobilization is as derived in laboratory observations, and that sand-sized particles and/or dust are infinitely available. Hence it is assumed that dust lifting is limited only by the ability of the atmosphere to generate wind of sufficient strength to initiate mobilization of sand-sized particles, and the dynamical processes leading to high wind stresses are examined. While it is evident that the availability of sand-sized particles will provide an important constraint on dust lifting in the aforementioned scenario, examination of that constraint is deferred to other studies in order to isolate dynamical constraints on dust lifting by mobilization of sand-sized particles. It is also apparent that dust lifting can occur by other mechanisms, for example, dust devils. These mechanisms should also be examined and would be complementary to this study.

[7] The focus of this study on cap edge dust lifting along the retreating edge of the southern spring polar cap is motivated by examination of newly acquired Mars Global Surveyor (MGS) Mars Orbiter Camera (MOC) [*Malin et al.*, 1992] color images and Thermal Emission Spectrometer (TES) [*Christensen et al.*, 1992] 9 μm dust optical depth measurements demonstrating dust activity near the south pole. The Mars Mesoscale Model (Mars MM5)/Geophysical Fluid Dynamics Laboratory (GFDL) Mars General Circulation Model (GCM) modeling system [*Toigo and Richardson*, 2002] is employed to address a number of significant questions relating to the lifting of dust near the south polar cap. These are as follows:

- Can the critical saltation-initiating stress threshold be exceeded?
- What scales of motion are important?
- What conditions create winds that exceed threshold (local time, cap temperature contrast, etc.)?
- Is there any dust feedback on lifting once dust is lofted?

[8] Descriptions of the models (section 2) are provided, and then some examples of cap edge dust storm systems observed by MGS (section 3) are shown. Samples of the MGS data are presented to provide motivation for the study by demonstrating that dust-lifting events do occur at this season and location and to show some examples of dust-lifting events, but the primary focus of this work is not on data analysis, but on mechanistic analysis of dust-lifting events using a high-resolution model. The behavior of the standard model is examined at three different seasonal dates with the specific goal of determining whether the surface wind stress threshold is exceeded (section 4). In section 5, circulation components most important for causing high surface stresses are isolated, specifically by examining the model simulation during mid southern summer. In section 6, dust injection is coupled to those locations where stress thresholds are exceeded in order to examine whether radiative/dynamical feedbacks associated with lofted dust enhance or diminish surface stresses. Finally, in section 7, conclusions are summarized.

2. Model Description

[9] In this study both the Mars Mesoscale Model (Mars MM5) and the GFDL Mars GCM are used. These models are briefly described here but are far more fully described by *Toigo and Richardson* [2002] and *Wilson and Hamilton* [1996], respectively.

[10] The GFDL Mars GCM is based on the GFDL "Skyhi" troposphere-stratosphere-mesosphere terrestrial model [*Hamilton et al.*, 1995]. The Mars GCM includes radiative heating due to CO_2 gas and atmospheric dust. Dust is treated within the model as a transportable (by model-resolved winds and diffusion) trace species leading to radiatively and dynamically self-consistent circulations. Two dust-particle sizes are considered, roughly 0.6 and 2.5 μm in radius. The background level of dust opacity is maintained by a dust injection scheme which triggers

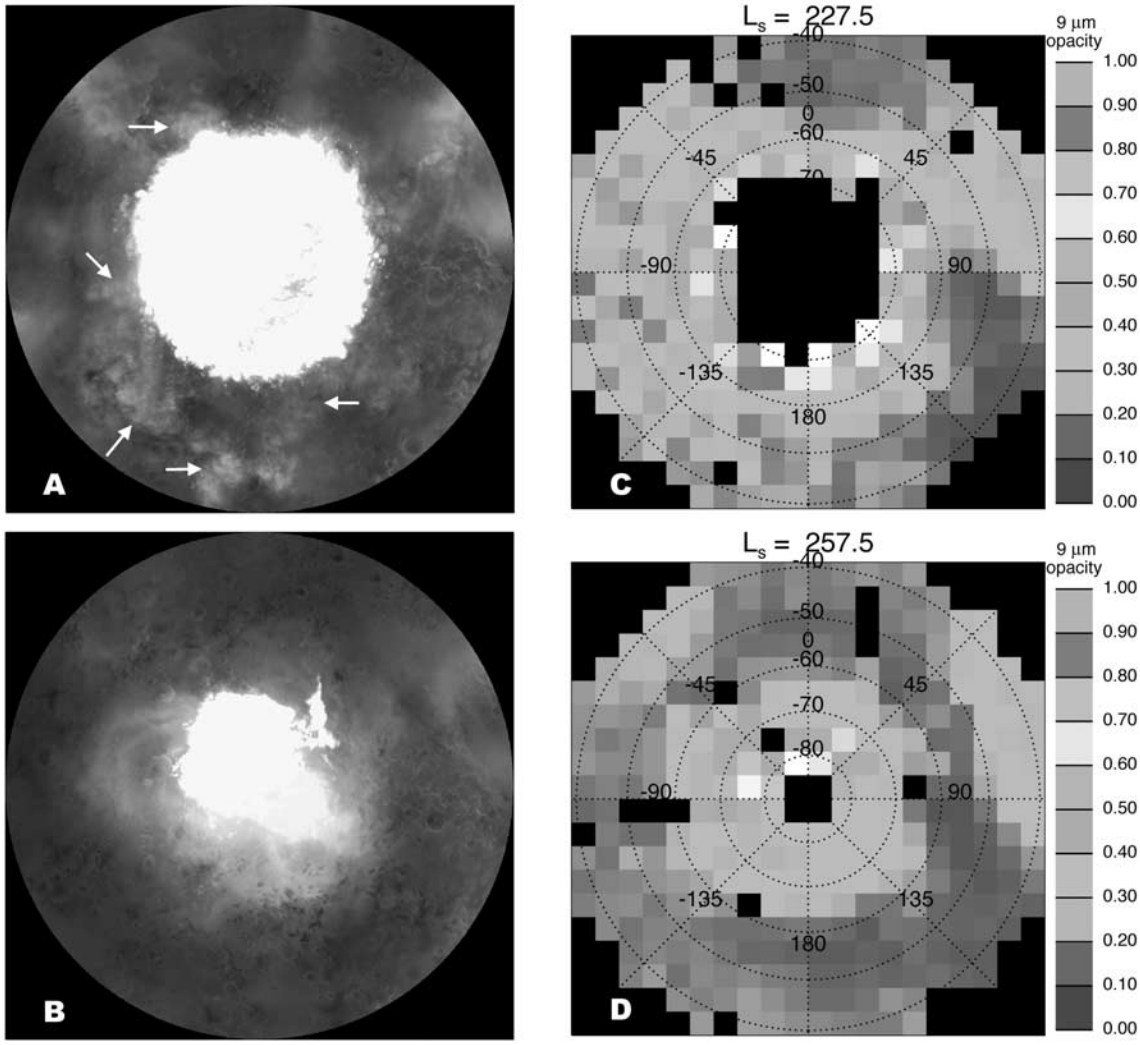

Figure 1. (a) MOC mosaic of the south pole at L_s = 228°. The outer edge of the image is at 45°S. The seasonal cap extends to about 68°S and is roughly circular. Yellow-brown dust clouds (next to the white arrows) can be seen all around the edge of the cap, and a large dust cloud (also indicated with an arrow) can be seen separate from the cap at the bottom of the map. (b) MOC mosaic of the south pole at L_s = 260°. The cap is now asymmetrical and more centered on its residual location. Diffuse dust is observed over the layered terrain region, and there is less evidence for discrete "puffy" clouds seen at L_s = 228°. Filamentary dust clouds are observed streaming off the cap edge in the left half of the map. (c) Map of TES-derived 9 μm opacities at L_s = 227.5°. Data are binned by 5° in L_s and in 5° boxes. (d) Same as Figure 1c, except at L_s = 257.5°. See color version of this figure at back of this issue.

injection of dust if the difference between the surface temperature and the lowest layer air temperature exceeds a critical value. The model also includes full CO_2 and water cycles (the exchange of CO_2 and water between the atmosphere and surface) [*Richardson*, 1999]. As used in this study, the model has a resolution of 5° in latitude and 6° in longitude with 20 vertical levels between the surface and roughly 85 km. The model is forced by a diurnal and seasonal cycle of incident solar radiation.

[11] The Mars Mesoscale Model is based on the widely used Pennsylvania State University/National Center for Atmospheric Research Fifth Generation Mesoscale Model (MM5) [*Dudhia*, 1993]. The Mars MM5 includes the same Martian-specific physical parameterizations as included in the GFDL Mars GCM, including the use of dust as an injected, transported, and radiatively active species. Being a limited-area model, the Mars MM5 requires specification of time-evolving boundary conditions, which are provided in the simulations discussed in this paper by output from the GCM at 2-hour intervals. The resolution of the Mars MM5 is variable. The resolution used in specific simulations in this study will be mentioned in the description of those simulations.

[12] For simulations employed in this study, the Mars GCM was "tuned" to match Viking and MGS observations on a global scale. Specifically, this involved prescribing a

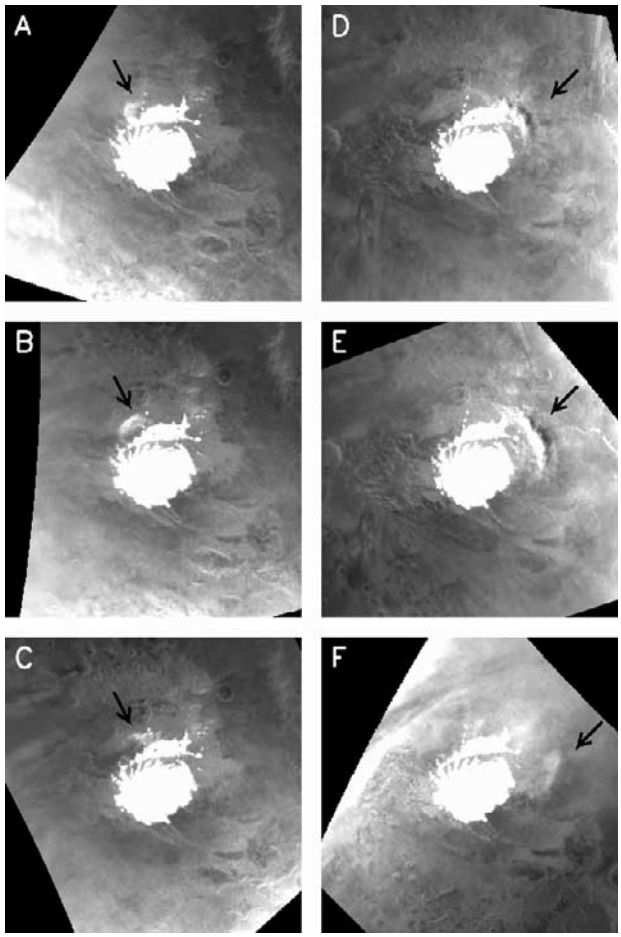

Figure 2. MOC images of dust activity over the south pole at $L_s = 310°$. Figures 2a–2c and 2d–2f each form a set of three images, with each image in the set separated by 2 hours (with one exception). The black arrows indicate the dust cloud. The clouds were not seen in the images just before Figures 2a and 2d. The dust clouds grow from the first to the second image and decay in the third. Eastward longitude increases clockwise in each subimage, with 0°E extending from the center of the image to the top. Local times at the center of the dust cloud (location of the black arrow) in each of the images are (a) 1000 LT, (b) noon, (c) 1400 LT, (d) 2200 LT, (e) midnight, and (f) noon.

fixed (spatially and temporally) dust injection rate that when used with the dust injection scheme, resulted in a seasonally evolving dust distribution that provided a good fit to tropical and global midlevel air temperatures, defined by the Viking Infrared Thermal Mapper (IRTM) 15 μm channel and the MGS TES standard temperature retrieval levels [see also *Wilson and Richardson*, 2000]. Simultaneously, the same dust injection scheme and rate allowed a good fit to midlevel tidal patterns in air temperature (which are best diagnosed from the Viking data due to superior local time coverage). In addition, the model predictions of the annual and tidal surface pressure records at the Viking and Mars Pathfinder lander locations were assessed, and the global atmospheric mass was adjusted so that a good fit was generated. Once adjusted, the model is able to produce a closed annual cycle (no interannual drift) over many Mars years. This GCM output was used as boundary and initial conditions for the Mars MM5, ensuring that the Mars MM5 simulations were consistent with spacecraft observations on the broadest scale.

[13] It is worth briefly discussing the interaction between the Mars MM5 and the Mars GCM. This issue is more comprehensively discussed by *Toigo and Richardson* [2002]. The Mars MM5 bulk atmospheric state is initially completely determined by the Mars GCM, and the winds and temperature at the boundaries of the Mars MM5 simulations continue to be driven by the Mars GCM. In the absence of structure (topography, ice boundary, albedo, etc.) in the MM5 domain beyond the resolution of the GCM, and in the absence of strong surface-atmosphere temperature contrasts (which tend to drive convective motions down to the resolution of the Mars MM5 simulation), the Mars MM5 and the Mars GCM simulations agree on the circulation within the Mars MM5 domain. For example, the Mars MM5 has been proven able to propagate baroclinic systems through its domain that are naturally generated in the Mars GCM [*Toigo and Richardson*, 2002]. Conversely, in the presence of strong surface structure or surface-atmosphere temperature contrasts, the Mars MM5 is readily able to modify the circulation within its own domain [*Toigo and Richardson*, 2001].

3. Mars Global Surveyor Observations of South Polar Cap Edge Dust Storms

[14] The Mars Global Surveyor spacecraft has provided systematic Sun-synchronous mapping of the Martian atmosphere and surface. This study utilizes the color MOC wide-angle global map swathes [*Malin et al.*, 1992], which can be mosaicked together to provide daily global maps showing dust activity, and the TES spectra [*Christensen et al.*, 1992], which can be used to derive 9 μm dust opacities. The combination of these two data sets provides a systematic and regular record of dust activity in the south polar region of Mars during spring and summer.

[15] Daily MOC images of the south polar region for southern spring and summer of the first MGS mapping year were created and examined [*Wang and Ingersoll*, 2002]. Selected examples showing dust activity are presented in Figure 1. The raw blue and red MOC images that make up these final image products were extracted from the Planetary Data System (PDS) CD-ROMs. Each image was radiometrically corrected to remove streaks and changes in the camera gain state while the image was being acquired. Then the images were photometrically corrected to remove large-scale brightness variations, due to the opposition surge, limb brightening (in the blue images), limb darkening (in the red images), and low-frequency camera sensitivity. The photometric corrections have the effect of equalizing the brightness across the whole image. The spacecraft ground track walks westward by 28° on each succeeding orbit and returns to approximately the same longitudes 1 day later after 13 orbits. The 13 red images were polar stereographically projected and mosaicked together to make one red daily polar map, and likewise for the blue. A composite daily color polar map was made by empirically mixing the red and blue images subject to the constraint that polar caps are "white." Two daily color polar maps are shown in Figure 1. These images were selected as the best examples of dust activity near the cap

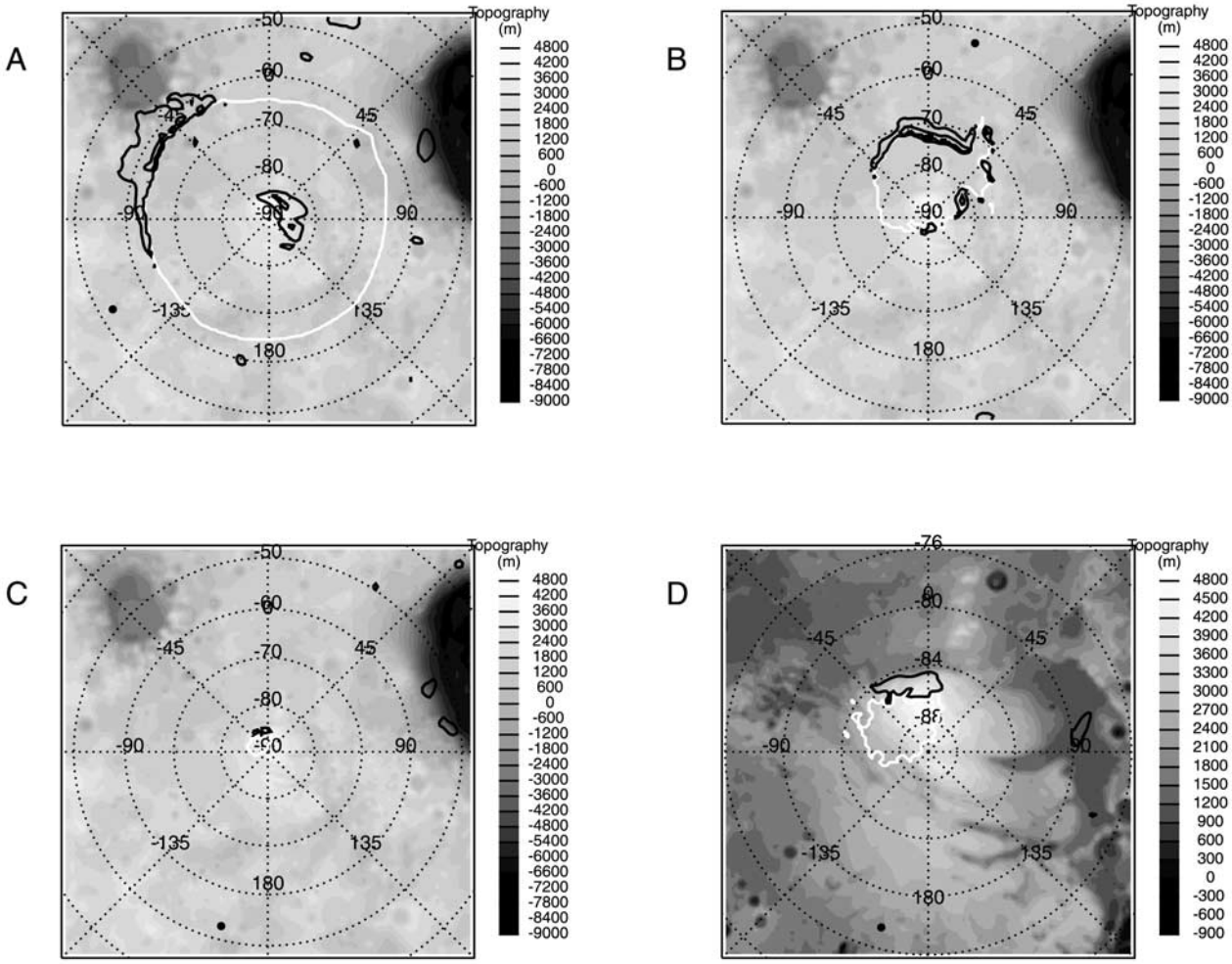

Figure 3. Maps of the south polar region used in the mesoscale simulations. Topography is shown by the gray shading in the background. The extent of the seasonal cap is shown by the white line. Surface wind stress is contoured by the thick black lines in intervals of 0.032 Pa. The small black circle is the longitude of local noon. (a) L_s = 225°. Local noon is at −120°E. (b) L_s = 255°. Local noon is at 15°E. (c and d) L_s = 310° (large and small domains used). Local noon is at −165°E.

edge while the cap was relatively large and circular (L_s = 228) (L_s is the angular measure of season for Mars, where L_s = 0 corresponds to northern spring equinox, L_s = 90 corresponds to northern summer solstice, etc.) and when the 9 μm dust optical depths were increasing (L_s = 260).

[16] The TES observations do not provide complete global coverage on a daily basis. Polar stereographic maps of TES observations are compiled in Figure 1 by binning and averaging over 5° of L_s. Individual daytime TES spectra were convolved with the Viking Infrared Thermal Mapper (IRTM) channel spectral response functions, and the resulting channel radiances were converted to brightness temperature. These IRTM-like (or synthetic IRTM) brightness temperatures are then used to calculate 9 μm optical depths following the method of *Martin* [1986], which are then directly comparable to those observed by Viking [*Martin*, 1986; *Martin and Richardson*, 1993]. The individual 9 μm optical depth measurements are binned in 240 km boxes in polar stereographic projection.

[17] Both the MOC images and the TES opacity maps show significant dust activity near the edge of the retreating south seasonal ice cap throughout mid and late southern spring. By late southern spring, dust is concentrated within 25° of the rotational pole. There is evidence for sporadic dust lifting at the cap edge throughout mid and late spring. The L_s = 228 image (Figure 1a) clearly shows a number of discrete well-defined dust clouds everywhere around the cap edge, especially in the lower left quadrant. By later in the season, the MOC images and the TES data show evidence for accumulation of dust. While the background dust away from this polar accumulation has characteristic 9μm optical depth of between 0.1 and 0.2, inside of the polar region the opacity can be in excess of 0.5. Combined, these data suggest the capability of cap-related wind systems to lift significant amounts of dust during these seasons.

[18] Typical midsummer dust activity (L_s = 310) is shown in Figure 2. At this season the dust activity near the south polar cap in general is much decreased, and the appearance of dust clouds is both smaller and much less frequent. In Figures 2a–2c (each separated in time by 2 hours), a small dust cloud is created near the edge of the polar cap, blows away from the cap, and then dissipates over a period of 6

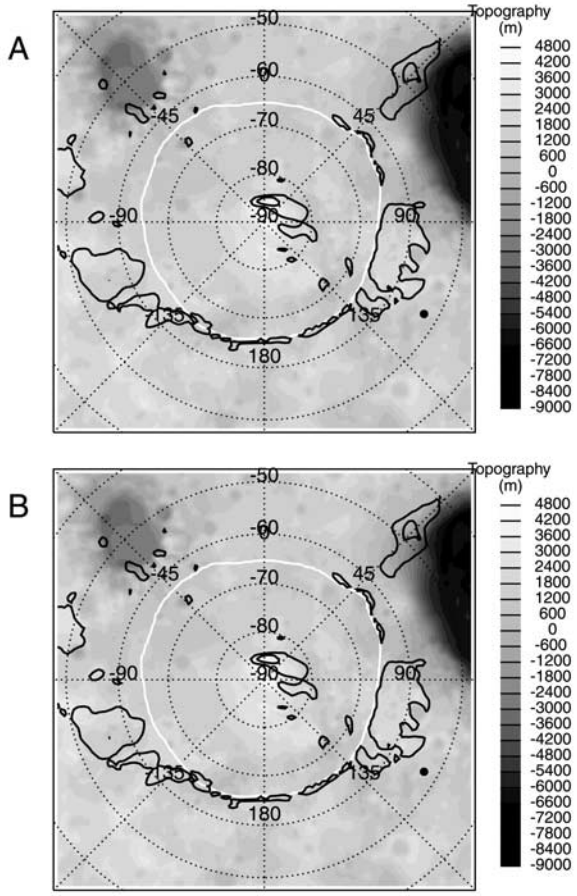

Figure 4. Wind stresses in the south polar region at L_s = 225°. Topography is shown by the gray shading in the background. The extent of the seasonal cap is shown by the white line. Surface wind stress is contoured by the thick black lines in intervals of 0.032 Pa. The small black circle is the longitude of local noon, in this case, 120°E. (a) "Base" simulation. (b) Simulation where the surface covering of CO_2 ice has been removed.

hours starting around 1000 local time (LT) (at the site of the cloud). In Figure 2d a slightly larger dust cloud appears off the edge of the cap. This occurs during the nighttime hours, ~2200 LT. (Here and elsewhere, we will continue to use the term "night" for the period when the Sun is lowest in the sky, despite the fact that at this season the Sun is obviously above the horizon all day in the polar regions.) In Figure 2e, 2 hours later, the cloud has grown somewhat larger and has moved away from the cap. Then, after a gap of 8 hours due to missing images, the cloud is seen to have decreased in both size and optical depth. Image sequences like these are typical of dust activity in midsummer near the south pole.

4. Occurrence and Location of Surface Stresses Sufficient to Initiate Dust Lifting

[19] The spacecraft observations of dust lifting in the polar regions, combined with theoretical arguments which suggest that surface winds should be elevated near the cap edge, provide strong motivation for the study of cap edge dust lifting in a three-dimensional numerical model. The importance of various factors that influence the circulation (and generation of high wind stresses), such as the CO_2 sublimation flow, topography, and the strong thermal contrast created by the cap edge, should also be tested.

[20] The first step in determining whether the model can reproduce observed dust activity near the south polar cap is to check whether the model can produce surface wind stresses of enough strength to initiate dust lifting by the criteria discussed in section 1. To this end, an experiment using Mars MM5 was conducted to simulate surface wind stresses in the south polar region at various points in the mid and late southern spring season. The highest-resolution topography [*Smith et al.*, 1999], thermal inertia [*Vasavada et al.*, 2000], and albedo [*Vasavada et al.*, 2000] data sets available and output from the GFDL Mars GCM, which was tuned to match the observations of atmospheric temperature, were employed in the model. Note that the Viking thermal inertia maps of the polar regions remain the best available due to the much superior Viking IRTM local time coverage. We use the Viking polar albedo maps from the same study to retain consistency in generating correct surface temperatures. The model domain was chosen to be centered on the south pole and extend out to 50°S, with a horizontal resolution of 40 km between grid points. For the simulation at L_s = 310, the cap was sufficiently small to warrant embedding another, higher-resolution domain, also centered on the south pole, with a horizontal resolution of ~13 km and extending out to 76°S. In both domains, there were 12 vertical levels from the surface to 40 km height, with the lowest layer centered at a height of 50 m. The south polar cap used in the L_s = 225 simulation is the Mars GCM-predicted cap. However, for the L_s = 255 and L_s = 310 simulations the cap is small enough that the latitudinal resolution of the GCM (~300 km) is too large to allow for accurate modeling of the cap shape. In these Mars MM5 simulations the GCM-predicted cap is overwritten with a cap defined by Viking images of the south polar cap at the relevant season.

[21] The wind stress maps for the three simulations (L_s = 225°, 255°, and 310°) are shown in Figure 3. In each case, times of day when high wind stresses covered the greatest area were selected. The figures show areas of the surface for which the stress exceeds a value of 0.032 Pa. This value was chosen to be the dynamic stress threshold on the basis of the laboratory assessment of 0.04 Pa as the static stress threshold for saltation. The value corresponds to those used in some studies [*Iversen et al.*, 1976; *Anderson et al.*, 1999], as well as being in the midrange of values derived from others [*White*, 1979; *Greeley et al.*, 1980]. The static threshold is the stress required to initiate motion of sand-sized particles. The dynamic threshold is the stress necessary to sustain motion after it has been initiated. The dynamic threshold is roughly 80% of the static value based on observations [*Bagnold*, 1941]. The dynamic threshold was chosen for use on the assumption that sub-grid-scale winds will exceed the static threshold in grid boxes where the dynamic threshold is exceeded (and that if the static threshold is exceeded by gusts in a grid box whose average wind stress does not exceed the dynamic value, any dust lifted will quickly dissipate). In three seasonal cases examined, significant areas of the model domain exceed the chosen threshold. In fact, if 0.04 Pa had been chosen, much of these areas would still have exceeded threshold.

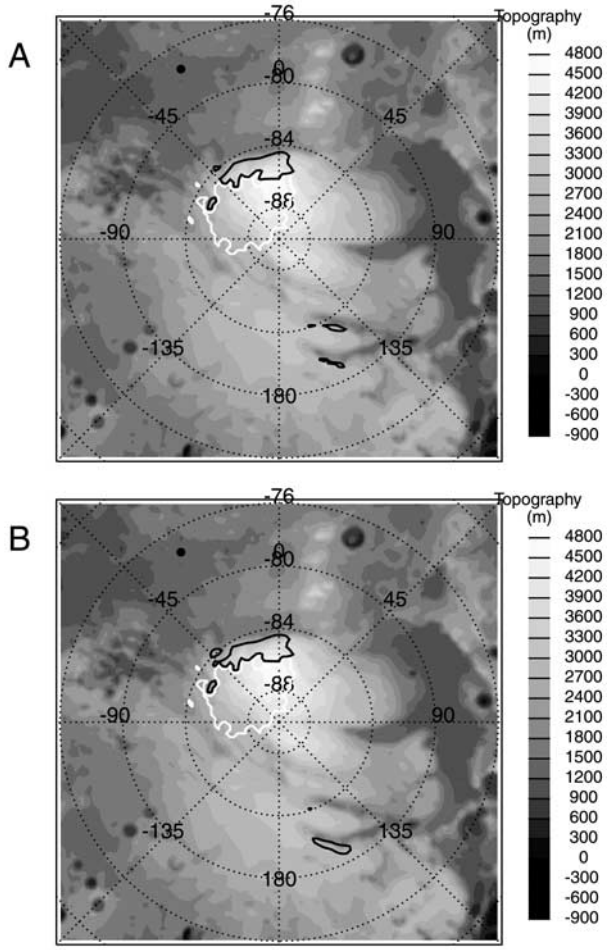

Figure 5. Wind stresses in the south polar region at L_s = 310°. Topography is shown by the gray shading in the background. The extent of the seasonal cap is shown by the white line. Surface wind stress is contoured by the thick black lines in intervals of 0.032 Pa. The small black circle is the longitude of local noon, in this case, −30°E. (a) "Base" simulation. (b) Simulation where the surface covering of CO_2 ice has been removed.

[22] The three seasonal dates for which simulations were conducted, L_s = 225°, 255°, and 310°, were chosen for two primary reasons. First, the different dates correspond to different extents of the seasonal ice cap, from extensive and nearly circular at L_s = 225° to approximately the residual extent at L_s = 310. Second, the observations show that in the midspring season, there was significant discrete cap edge storm behavior, while a buildup of dust in the polar regions occurred after L_s = 255°. Thus the observations suggest that this set of simulations should provide a range of polar dust-lifting behavior. In the following paragraphs the results of the simulations are described in seasonal order. Given that the simulations exhibit a great deal of time variability, it is not possible to capture this range of behavior in figures. This variability is mostly with respect to variations in local time; day-to-day variations (throughout the extent of the model run) in location and extent of regions of high wind stress are negligible. However, to provide some idea of the occurrence and behavior of dust lifting, Figure 3 shows representative time snapshots of the simulations. Note that the term "lifting" will be used in this section to denote occurrences of surface wind stresses exceeding the dynamic threshold.

[23] For L_s = 225° the simulation shows a great deal of lifting along the cap edge (Figure 3a). Lifting occurs at all longitudes at some point during the day. Right at the cap edge, lifting is roughly in phase with the Sun, with significant cap edge lifting occurring generally between the local times of approximately noon and 1800 LT. In these cases, lifting occurs right at the very edge of the cap. However, significant lifting also occurs during the night and morning in certain longitude regions. Specifically, significant non-afternoon lifting occurs in the region between −30°E and −60°E within 10° of the cap edge and in the region between 45°E and 90°E between 2° and 10° from the cap edge. Between 90°E and 135°E, significant lifting occurs right at the cap edge and extending out by over 15° of latitude beginning at 0600 LT and continuing to ∼1900 LT.

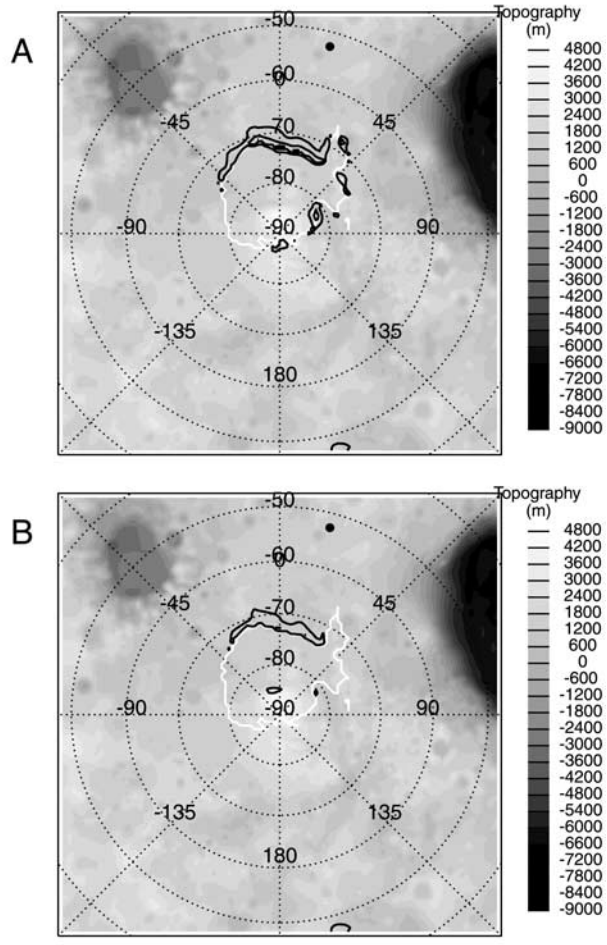

Figure 6. Wind stresses in the south polar region at L_s = 255°. Topography is shown by the gray shading in the background. The extent of the seasonal cap is shown by the white line. Surface wind stress is contoured by the thick black lines in intervals of 0.032 Pa. The small black circle is the longitude of local noon, in this case, 15°E. (a) "Base" simulation. (b) Simulation where the surface covering of CO_2 ice has been removed.

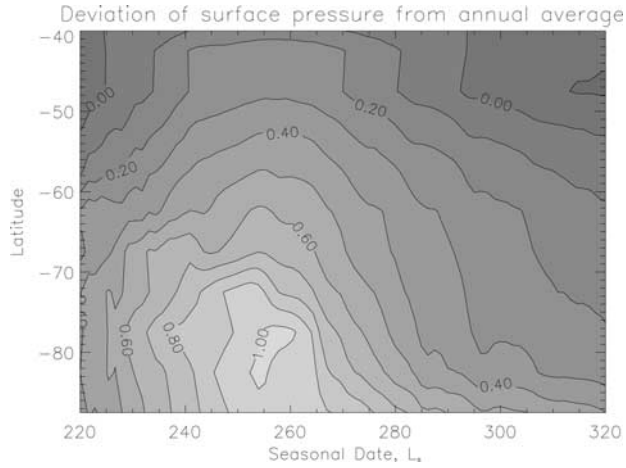

Figure 7. Evolution of surface pressure gradients across the polar cap edge during southern spring and early southern summer from the Mars GCM. The deviation of the zonal-average surface pressure from the annual (so as to remove topographic effects) and zonally averaged surface pressure in each latitude band is shown as a function of latitude and season. The units are in millibars. The plot shows that the pressure gradient is a maximum at roughly L_s = 255°, with a drop of about 0.75 mbar between 85°S and 45°S. By contrast, the pressure drop across the same latitude range is 0.5 mbar at L_s = 225° and 0.4 mbar at L_s = 310°. Also, the maximum gradients across the cap edge are 0.05 mbar/degree at L_s = 255° versus <0.02 mbar/degree at L_s = 225° and 310°.

[24] A major qualitative change in the behavior of dust lifting occurs between the L_s = 225° and 255° simulations (Figure 3b). Lifting no longer occurs at every longitude at least once during the day. Lifting is now present primarily at the immediate cap edge between 60°E and −90°E. This may be related to the fact that the cap is no longer circular. Lifting occurs between the local times of 0700 and 2200, with maximal extent during the early afternoon. Small areas of additional lifting occur on the polar layered terrains, centered at 180°E between 1900 LT and midnight, and in a "bay" of defrosted ground surrounded by seasonal ice cap on three sides, at 60°E and 82°S, with lifting occurring at all times during the day. In addition, a small but persistent region of dust lifting is in Chasma Australe in predawn morning (∼0400 LT). This dust lifting is likely associated with nighttime drainage flow off the seasonal cap. Despite the fact that the Sun is up all "night" by this point in the year in the south polar regions, there remains a diurnal cycle of heating as the elevation of the Sun in the sky proceeds on its daily cycle. This muted cycle is still able to drive slope winds and tidal rotation of the wind vectors.

[25] By L_s = 310° the region of cap edge lifting has shrunk to between 0°E and −45° E (Figures 3c and 3d). The cap in this simulation is essentially the residual cap. Lifting of roughly similar intensity and duration occurs during two periods. The first period of lifting is centered on the noon hours, as in the earlier seasonal date simulations, but for a small range of local times, between 0800 and 1400 LT. Strongest stresses during this period occur around local noon. The second lifting period occurs during the night, between the hours of 2000 and 0200 LT, with strongest stresses around 2300 LT.

5. Causes of High Surface Wind Stresses

[26] Having determined that the critical stress is exceeded, experiments designed to examine which components of the dynamical system (slopes, thermal contrast, thermal tides, etc.) are dominant in generating the high wind stresses were conducted. In order to isolate dynamical forcings, simulations were designed in which the CO_2 sublimation flow was deactivated, in which the thermal effects of the cap were removed (i.e., ice and differences in thermal inertia and albedo), in which the topography of the south polar region was flattened, and, finally, in which both the topography was flattened and the thermal effects of the cap were removed. Because of the large number of simulations

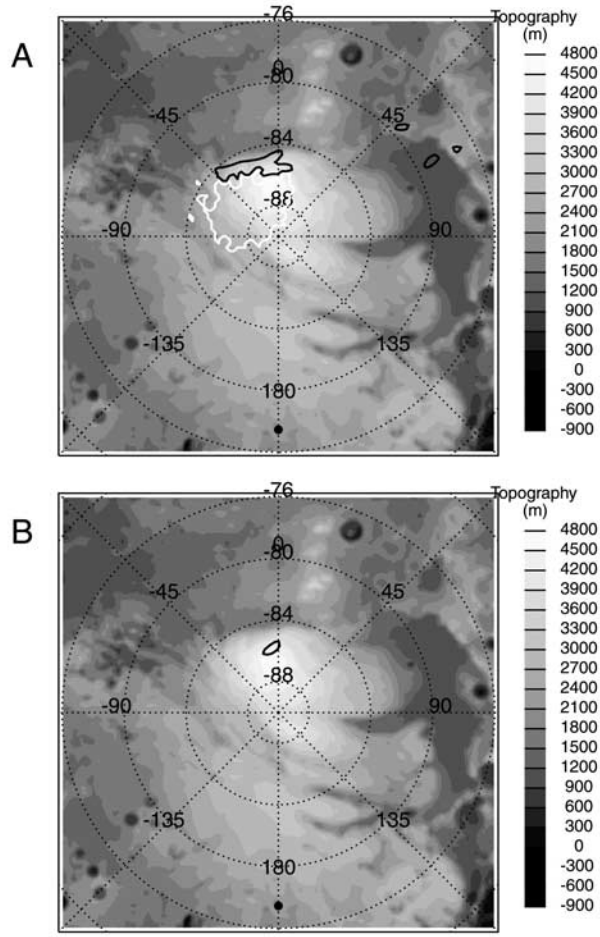

Figure 8. Wind stresses in the south polar region at L_s = 310°. Topography is shown by the gray shading in the background. The extent of the seasonal cap is shown by the white line. Surface wind stress is contoured by the thick black lines in intervals of 0.032 Pa. The small black circle is the longitude of local noon, in this case, 180°E. (a) "Base" simulation. (b) Simulation where the thermal effects of the residual cap (i.e., CO_2 ice, thermal inertia, and albedo signature) have been removed.

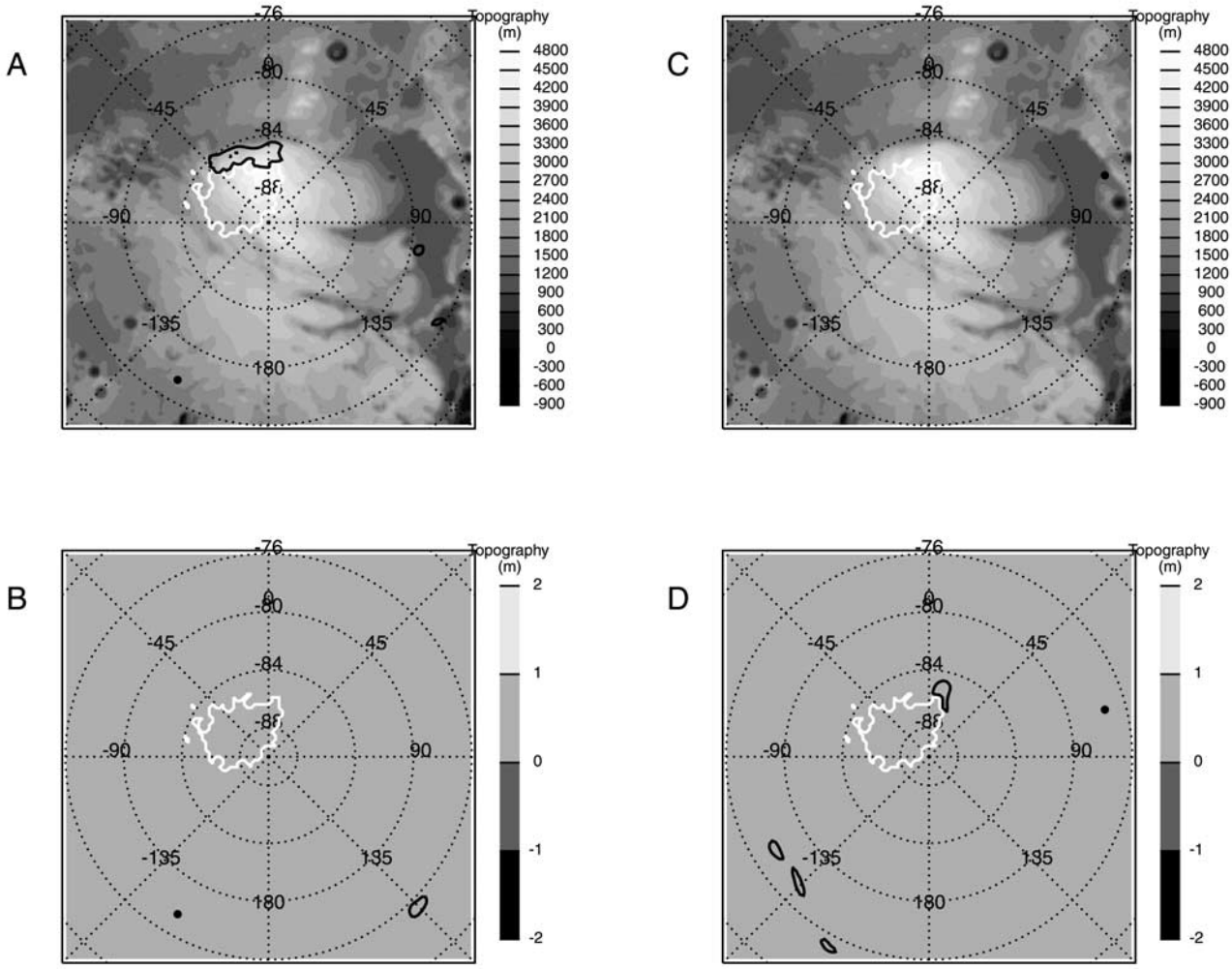

Figure 9. Wind stresses in the south polar region at L_s = 310°. Topography is shown by the gray shading in the background. The extent of the seasonal cap is shown by the white line. Surface wind stress is contoured by the thick black lines in intervals of 0.032 Pa. The small black circle is the longitude of local noon. (a) ''Base'' simulation. Local noon is at −150°E. (b) Simulation with no topography, highlighting the loss of cap edge lifting between 0°E and −45°E at the same instant of time as Figure 9a. (c) ''Base'' simulation. Local noon is at 75°E. (d) Simulation with no topography, highlighting the new area of cap edge lifting between 0°E and 30°E that is not seen at the same instant of time as Figure 9c.

required to elucidate dynamical processes, these simulations were undertaken at only one seasonal date. As the mid-spring (L_s = 225°) simulation is likely dominated by the great areal extent of the seasonal cap and the thermal effects of the cap edge, we decided to concentrate on the mid-summer (L_s = 310°) period, where the effect of topography should be greatest. Again, in this section the term ''lifting'' will be used to denote occurrences of surface wind stresses exceeding the dynamic threshold.

[27] Only for the tests to determine the influence of the CO_2 sublimation flow (the flow of air away from the polar cap due to sublimation of the CO_2 ice) were simulations performed at all three seasonal dates. This was done to determine the influence of the size of the seasonal cap on wind as well. The results for L_s = 225° are shown in Figure 4. There is essentially no difference in either the magnitude or location of high wind stresses during this season. The same is true for the cap at L_s = 310°, as shown in Figure 5. Again, the locations, periods, and magnitudes of high wind stress are almost identical between the base simulation and the simulation with sublimation flow deactivated. At these two times it would appear that the condensation flow is not particularly important in generating large surface winds. However, at L_s = 255° (Figure 6), there is a noticeable effect, though still small. Stresses are generally smaller with the condensation flow turned off. Locations of high wind stress are similar, but their areal extent is also smaller.

[28] The reason for the local maximum in sublimation wind impact at L_s = 255° can be seen in Figure 7, showing the pressure gradient across the southern polar region in the GCM. The pressure gradient, generated by the sublimation of CO_2 and consequently the dynamical drive for the CO_2 sublimation wind, has a maximum value at roughly L_s = 255°. This corresponds to the optimum combination of incident solar radiation and available CO_2 ice for sublimation.

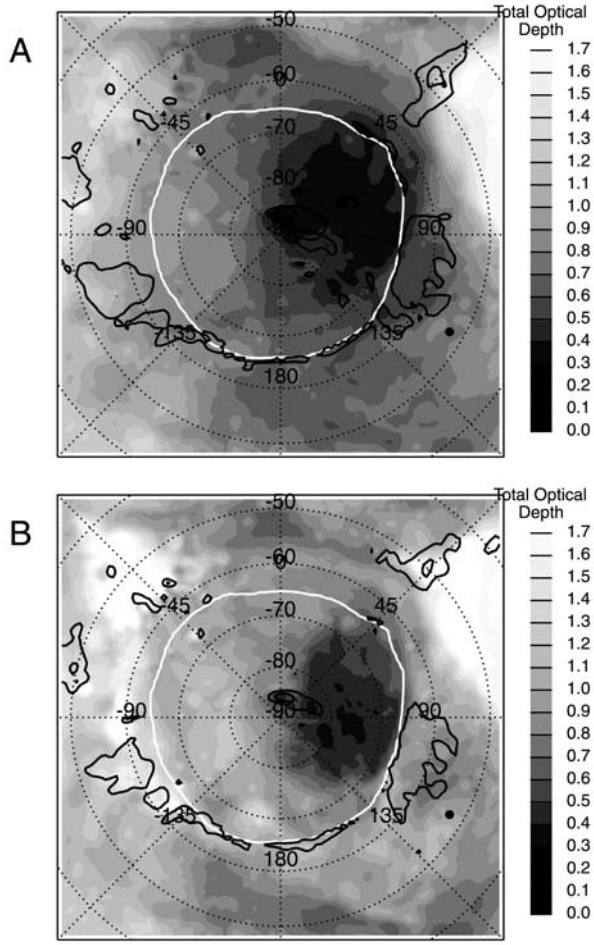

Figure 10. Wind stresses and optical depth in the south polar region at L_s = 225°. Optical depth is shown by the gray shading in the background. The extent of the seasonal cap is shown by the white line. Surface wind stress is contoured by the thick black lines in intervals of 0.032 Pa. The small black circle is the longitude of local noon, in this case, 120°E. (a) "Base" simulation. (b) Simulation with dust feedback. Small dust clouds (of high optical depth) can be seen near the cap edge. The large dusty areas to the upper left and upper right of the figure are Argyre and Hellas Basins being filled with dust.

[29] The effect of the thermal contrast between the cold, bright cap and the warmer, darker, defrosted surrounding terrain should give rise to a "sea breeze" circulation at the cap edge. The importance of this direct thermal contrast is examined by eliminating the cap thermal signature. This was accomplished by first removing the surface CO_2 ice and second replacing the polar cap thermal inertia and albedo values with the average of the surrounding terrain. A snapshot of the results is shown in Figure 8 in comparison to the "base" case. Cap edge lifting is almost entirely eliminated, reinforcing the idea that these winds are directly related to the thermal contrast. One very slight exception is provided by the region of strongest slope on the edge of the layered deposits between 0°E and −45°E. At approximately local midnight a short period (∼2 hours) of lifting occurs, likely associated with strong downslope winds. Winds away from the immediate vicinity of the cap are largely unaffected by the removal of the cap thermal signature. This suggests that the high wind speeds and wind stresses are being controlled by a forcing different than thermal contrast.

[30] A further simulation was conducted whereby the topography was flattened uniformly in the south polar region to a height of 0 km (the MOLA reference elevation). The thermal effects of the cap were present in this simulation along with spatial variations in albedo and thermal inertia throughout the model domain. Figure 9 shows the comparison between this simulation and the "base" case. The cap edge lifting occurring at the region of maximum slope now disappears (Figures 9a and 9b). A new location of cap edge lifting occurs between 0°E and 45°E, during the period between 0900 and 1300 LT (Figures 9c and 9d).

6. Dust Feedback on Dust Lifting

[31] So far, surface wind stresses have been examined in isolation from any potential feedback between the radiative effects of lofted dust and the surface winds. The question of whether dust-lifting events involve significant positive feedback is an important one within the context of dust storm generation. In this section the atmospheric injection of dust in the model is coupled to the prediction of surface wind stresses in excess of the dynamic threshold. Atmospheric heating due to dust is already included in the model. Any impact of the lofted dust on the surface stresses is examined. The prescription of dust injection is relatively simple: if the surface wind stress in a grid box is above threshold, a surface-to-lowest-level dust flux is augmented. In a given simulation the rate of injection while the stress is above threshold is constant. This is likely not what happens in reality, that is, higher stresses inject more dust, but this relation was chosen as a simple first approximation. As mentioned in section 2, the GFDL Mars GCM and the Mars MM5 prescribe a background dust injection rate in order to maintain a background distribution of dust necessary to match observations of air temperatures. In the Mars MM5 simulations described in this section, when the threshold is exceeded, dust is injected at a rate of between 100 and 1000 (depending on the simulation) times this background rate. If the injection rate was too high, the entire domain filled with dust, up to optical depths of 10 or more, producing obviously unphysical situations (the optical depths observed were <1 in the 9 μm region, corresponding to visible values of 2−2.5). Only in these extreme simulations was any positive feedback on dust lifting observed (Figure 10).

[32] Figure 10 shows snapshots of simulations at L_s = 225° both without and with dust injection. The background gray shading shows the optical depth of the atmosphere, and the black lines show regions where the wind stress exceeds 0.032 Pa. The regions of high stress are the sites where small dust clouds develop in Figure 10b. Wisps of dust trail away from these locations, and filamentary dust clouds from previous injection events abound within the domain. Some amount of the injected dust is blown over the seasonal ice cap. While the very fine structure of the clouds observed in the MOC image (Figure 1a) is not apparent, this primarily results from the limitations of resolution. Dust is seen at most longitudes around the cap, as seen in the MOC image (Figure 1a). The presence of the thick dust clouds does not

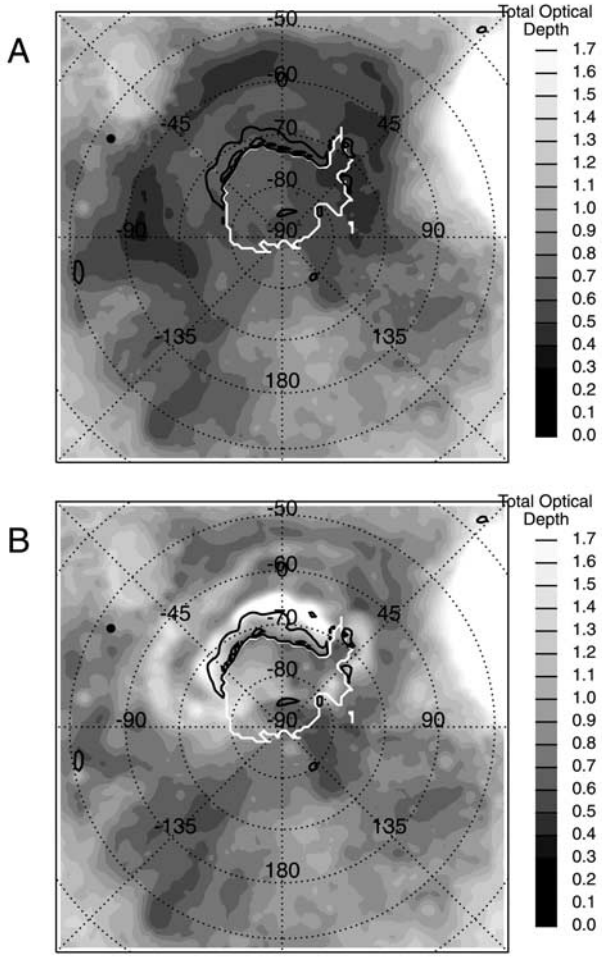

Figure 11. Wind stresses and optical depth in the south polar region at L_s = 255°. Optical depth is shown by the gray shading in the background. The extent of the seasonal cap is shown by the white line. Surface wind stress is contoured by the thick black lines in intervals of 0.032 Pa. The small black circle is the longitude of local noon, in this case, −60°E. (a) "Base" simulation. (b) Simulation with dust feedback. Dust clouds of high optical depth are being created at the edge of the cap, and the previous day's cloud can be seen slightly northward of the cap, although being less optically thick. Typically, only two "filaments" of dust clouds like this are seen at one time; they are created once every day, and the decay of the cloud back to background levels of optical depth takes about 1 day.

significantly alter the peak values or areal extent of the regions of high wind stress.

[33] The dominant pattern of dust injection and transport at L_s = 255° (Figure 11b, compared to Figure 11a) is that of the daily injection of dust along the cap edge between 60°E and −90°E. These daily bands of dust are advected by the circulation, resulting in concentric filamentary structures. There is some evidence in the MOC image (Figure 1b) for such multiply banded filamentary structures. However, the accumulation of dust in the 120°–180°E region over the polar layered terrain does not develop, as was observed in the MOC image. Again, the presence of the thick dust clouds does not significantly alter the peak values or areal extent of the regions of high wind stress.

[34] The extent of regions of dust lifting has shrunk by L_s = 310° (Figure 12). The dust injection rate used is twice that used in the L_s = 255° simulation discussed above. Using the same rate as the L_s = 255° produced clouds of optical depth only marginally greater than the background value and of very short duration (<2 hours). Even with the higher dust injection rate, fewer and smaller dust clouds are generated as compared to that period. In this simulation, dust is primarily injected at the cap edge between 0°E and −45°E, similar to the source location of the cloud seen in Figures 2a–2c. Dust clouds move away from the cap after generation, moving radially outward about 4–6 degrees of latitude before being advected eastward. Dust clouds decay

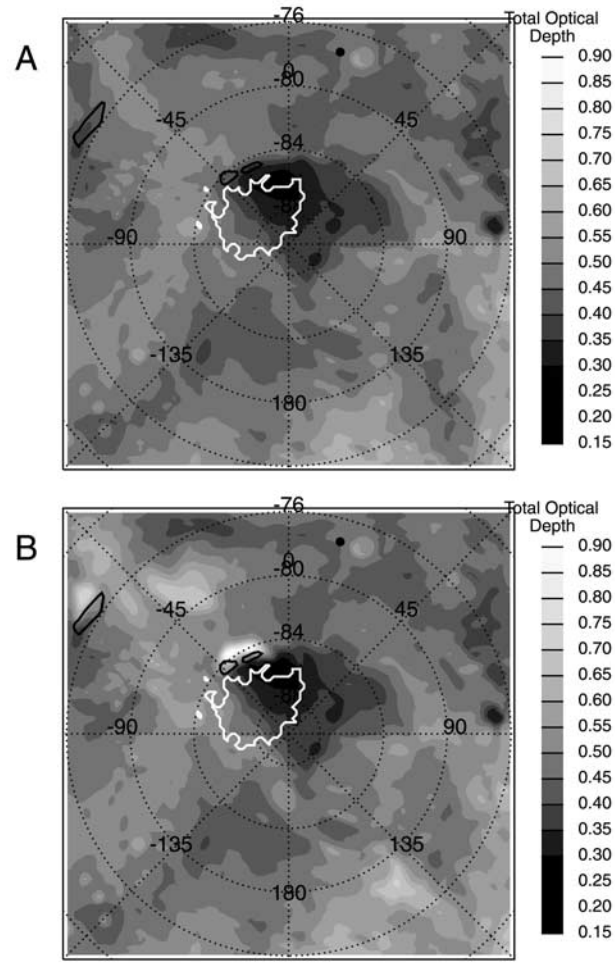

Figure 12. Wind stresses and optical depth in the south polar region at L_s = 310°. Optical depth is shown by the gray shading in the background. The extent of the seasonal cap is shown by the white line. Surface wind stress is contoured by the thick black lines in intervals of 0.032 Pa. The small black circle is the longitude of local noon, in this case, 15°E. (a) "Base" simulation. (b) Simulation with dust feedback. Dust clouds of high optical depth are being created at the edge of the cap between 0°E and −45°E. Comparing Figures 12a and 12b shows that the areas of high wind stress are not affected by the dust feedback.

to the background level of optical depth in about 1 day. No clouds were observed to be generated at the edge of the cap seen as the source for the cloud in Figures 2d–2f.

[35] In all of the seasonal cases described above, there is no consistent evidence for positive feedback on dust lifting, as gauged by examination of the areal extent of the regions of high wind stress. The simulations were carried out for 10 Mars days, and at the end of that period, the dust injection simulations produced nearly identical surface wind stress patterns to those in the "base" cases. The similarity of surface wind stress patterns between the "base" cases and the "feedback" simulations can be seen in Figures 10, 11, and 12. Thus it would appear for the case of dust lifting near the south polar cap during the late spring season, which primarily results from cap thermal contrasts and slope winds, that radiative dynamical feedbacks are not particularly important in the maintenance and generation of local dust storms.

7. Conclusions

[36] Mesoscale atmospheric simulations of the Martian high-latitude southern hemisphere during late spring have shown the occurrence of surface wind stresses in excess of the critical saltation-initiating value at a variety of locations and local times. The late southern spring period was focused on because of the availability of high-quality observations from the Mars Global Surveyor spacecraft, both from MOC images and from 9 μm dust opacities derived from TES observations. These data show dust activity near and over the cap and at the cap edge during this season.

[37] The mesoscale simulations readily generate surface wind stresses that exceed minimum saltation threshold in the regions where dust activity is observed in the MGS data during similar seasonal dates. Many, but not all, of these regions correspond to the immediate cap edge region. In this paper, cap edge wind systems are specifically examined. During the L_s = 225° simulation, high wind stresses are observed all around the cap edge during local afternoon hours. The L_s = 255° and 310° simulations show high wind stresses more restricted in physical location, although peak wind stresses still occur during the local afternoon hours. The L_s = 310° simulation also begins to show significant nighttime high wind stresses, in the same location that was active during afternoon hours in the L_s = 255° and 310° simulations.

[38] By eliminating forcing elements from the model, the important dynamical modes generating the high wind stresses at this season were isolated. The cap edge thermal contrast with ice-free bare ground provides the primary drive for high surface wind stresses in the cap edge region. In some locations, topographic slopes augment these cap edge winds. Sublimation flow due to the seasonal shrinking of the cap does not appear to play an important role either when the seasonal cap is very large or very small. However, the presence of sublimation flow during late southern spring (L_s = 255°) increases the winds and wind stresses at the cap edge.

[39] Further simulations in which the presence of high wind stresses are linked causally to the injection of large dust loads produce similar dust activity and dust cloud morphology to that observed in the MGS data at similar seasonal dates. No evidence for consistent positive or negative feedback from the radiative effects of dust clouds of moderate opacity ($\tau \approx 2$) thus created is observed on the surface wind stress fields in the simulations during this season.

[40] **Acknowledgments.** We would like to thank Mike Smith and an anonymous reviewer for useful comments and suggestions.

References

Anderson, F. S., R. Greeley, P. Xu, E. Lo, D. G. Blumberg, R. M. Haberle, and J. R. Murphy, Assessing the Martian surface distribution of aeolian sand using a Mars general circulation model, *J. Geophys. Res.*, *104*, 18,991–19,002, 1999.

Bagnold, R. A., *The Physics of Blown Sand and Desert Dunes*, Methuen, New York, 1941.

Burk, S. D., Diurnal winds near the Martian polar caps, *J. Atmos. Sci.*, *33*, 923–939, 1976.

Christensen, P. R., et al., Thermal Emission Spectrometer Experiment: Mars Observer Mission, *J. Geophys. Res.*, *97*, 7719–7734, 1992.

Dudhia, J., A nonhydrostatic version of the Penn State-NCAR mesoscale model: Validation tests and simulation of an Atlantic cyclone and cold front, *Mon. Weather Rev.*, *121*, 1493–1513, 1993.

Gierasch, P. J., and R. M. Goody, A model of a Martian great dust storm, *J. Atmos. Sci.*, *30*, 169–179, 1973.

Greeley, R., Silt-clay aggregates on Mars, *J. Geophys. Res.*, *84*, 6248–6254, 1979.

Greeley, R., and J. D. Iversen, *Wind as a Geological Process on Earth, Mars, Venus, and Titan*, Cambridge Univ. Press, New York, 1985.

Greeley, R., R. Leach, B. R. White, J. D. Iversen, and J. B. Pollack, Threshold windspeeds for sand on Mars: Wind tunnel simulations, *Geophys. Res. Lett.*, *7*, 121–124, 1980.

Greeley, R., N. Lancaster, S. Lee, and P. Thomas, Martian aeolian process, sediments and features, in *Mars*, edited by H. H. Kieffer et al., pp. 730–766, Univ. of Ariz. Press, Tucson, 1992.

Haberle, R. M., C. B. Leovy, and J. B. Pollack, A numerical model of the Martian polar cap winds, *Icarus*, *39*, 151–183, 1979.

Hamilton, K., R. J. Wilson, J. D. Mahlman, and L. J. Umscheid, Climatology of the SKYHI troposphere-stratosphere-mesosphere general circulation model, *J. Atmos. Sci.*, *52*, 5–43, 1995.

Iversen, J. D., J. B. Pollack, R. Greeley, and B. R. White, Saltation threshold on Mars: The effect of interparticle force, surface roughness, and low atmospheric density, *Icarus*, *29*, 381–393, 1976.

James, P. B., J. L. Hollingsworth, M. J. Wolff, and S. W. Lee, North polar dust storms in early spring on Mars, *Icarus*, *138*, 64–73, 1999.

Kahn, R. A., T. Z. Martin, R. W. Zurek, and S. W. Lee, The Martian dust cycle, in *Mars*, edited by H. H. Kieffer et al., pp. 1017–1053, Univ. of Ariz. Press, Tucson, 1992.

Leovy, C. B., R. W. Zurek, and J. B. Pollack, Mechanisms for Mars dust storms, *J. Atmos. Sci.*, *30*, 749–762, 1973.

Malin, M. C., G. E. Danielson, A. P. Ingersoll, H. Masursky, J. Veverka, M. A. Ravine, and T. A. Soulanille, Mars Observer Camera, *J. Geophys. Res.*, *97*, 7699–7718, 1992.

Martin, T. Z., Thermal infrared opacity of the Mars atmosphere, *Icarus*, *66*, 2–21, 1986.

Martin, T. Z., and M. I. Richardson, New dust opacity mapping from Viking infrared thermal mapper data, *J. Geophys. Res.*, *98*, 10,941–10,949, 1993.

Metzger, S. M., J. R. Carr, J. R. Johnson, T. J. Parker, and M. T. Lemmon, Dust devil vortices seen by the Mars Pathfinder camera, *Geophys. Res. Lett.*, *26*, 2781–2784, 1999.

Murphy, J. R., The Martian atmospheric dust cycle: Insights from numerical model simulations, in *The Fifth International Conference on Mars* [CD-ROM], abstract 6087, *LPI Contrib. 972*, Lunar and Planet. Inst., Houston, Tex., 1999.

Peterfreund, A. R., and H. H. Kieffer, Thermal infrared properties of the Martian atmosphere, 3, Local dust clouds, *J. Geophys. Res.*, *84*, 2853–2863, 1979.

Renno, N. O., A. A. Nash, J. Lunine, and J. Murphy, Martian and terrestrial dust devils: Test of a scaling theory using Pathfinder data, *J. Geophys. Res.*, *105*, 1859–1866, 2000.

Richardson, M. I., A general circulation model study of the Mars water cycle, Ph.D. thesis, Univ. of Calif., Los Angeles, 1999.

Siili, T., R. M. Haberle, and J. R. Murphy, Sensitivity of Martian southern polar cap edge winds and surface stresses to dust optical thickness and to the large-scale sublimation flow, *Adv. Space Res.*, *19*, 1241–1244, 1997.

Siili, T., R. M. Haberle, J. R. Murphy, and H. Savijärvi, Modelling of the

combined late-winter ice cap edge and slope winds in Mars' Hellas and Argyre regions, *Planet. Space Sci.*, *47*, 951–970, 1999.

Smith, D. E., et al., The global topography of Mars and implications for surface evolution, *Science*, *284*, 1495–1503, 1999.

Thomas, P., and P. J. Gierasch, Dust devils on Mars, *Science*, *230*, 175–177, 1985.

Toigo, A. D., and M. I. Richardson, The Mars exploration rovers: A meteorological tale of four landing sites, *Bull. Am. Astron. Soc.*, *33*, 1089, 2001.

Toigo, A. D., and M. I. Richardson, A mesoscale model for the Martian atmosphere, *J. Geophys. Res.*, *107*, 10.1029/2000JE001489, in press, 2002.

Vasavada, A. R., J.-P. Williams, D. A. Paige, K. E. Herkenhoff, N. T. Bridges, R. Greeley, B. C. Murray, D. S. Bass, and K. S. McBride, Surface properties of Mars' polar layered deposits and polar landing sites, *J. Geophys. Res.*, *105*, 6961–6970, 2000.

Wang, H., and A. P. Ingersoll, Martian clouds observed by Mars Global Surveyor Mars Orbiter Camera, *J. Geophys. Res.*, *107*, 10.1029/2001JE001815, in press, 2002.

White, B. R., Soil transport by winds on Mars, *J. Geophys. Res.*, *84*, 4643–4651, 1979.

Wilson, R. J., and K. Hamilton, Comprehensive model simulation of thermal tides in the Martian atmosphere, *J. Atmos. Sci.*, *53*, 1290–1326, 1996.

Wilson, R. J., and M. I. Richardson, The Martian atmosphere during the Viking Mission, 1, Infrared measurements of atmospheric temperatures revisited, *Icarus*, *145*, 555–579, 2000.

A. P. Ingersoll, M. I. Richardson, and H. Wang, Division of Geological and Planetary Sciences, MS 150-21, California Institute of Technology, Pasadena, CA 91125, USA.

A. D. Toigo, Center for Radiophysics and Space Research, Cornell University, 326 Space Sciences Building, Ithaca, NY 14853, USA. (toigo@astro.cornell.edu)

R. J. Wilson, NOAA/Geophysical Fluid Dynamics Laboratory, Princeton, NJ 08642, USA.

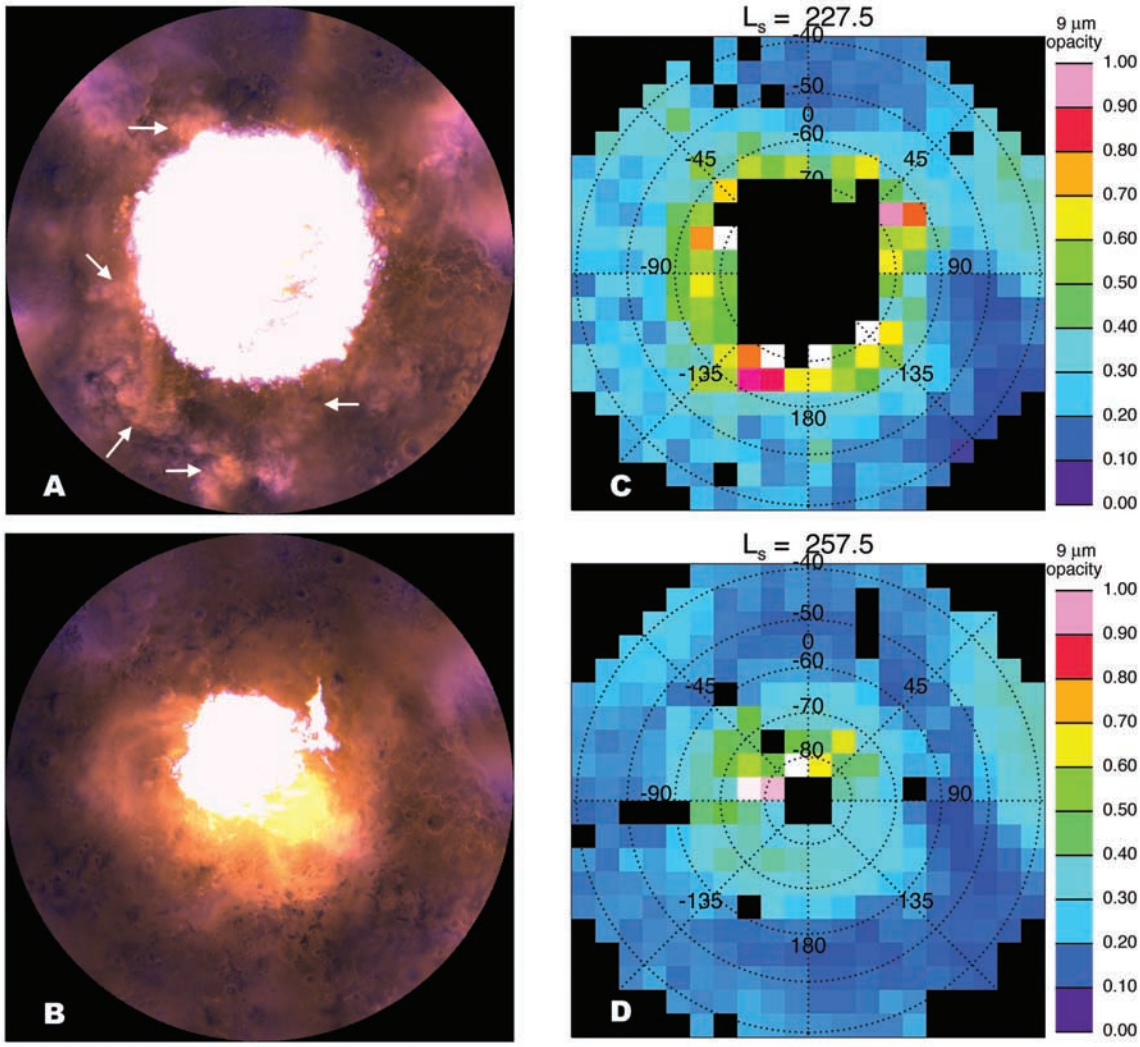

Figure 1. (a) MOC mosaic of the south pole at L_s = 228°. The outer edge of the image is at 45°S. The seasonal cap extends to about 68°S and is roughly circular. Yellow-brown dust clouds (next to the white arrows) can be seen all around the edge of the cap, and a large dust cloud (also indicated with an arrow) can be seen separate from the cap at the bottom of the map. (b) MOC mosaic of the south pole at L_s = 260°. The cap is now asymmetrical and more centered on its residual location. Diffuse dust is observed over the layered terrain region, and there is less evidence for discrete "puffy" clouds seen at L_s = 228°. Filamentary dust clouds are observed streaming off the cap edge in the left half of the map. (c) Map of TES-derived 9 μm opacities at L_s = 227.5°. Data are binned by 5° in L_s and in 5° boxes. (d) Same as Figure 1c, except at L_s = 257.5°.